

## **Supporting Information**

### **Near-infrared Light Manipulated Chemoselective Reductions Enabled by an Upconversional Supersandwich Nanostructure**

Zi-en Liu<sup>a,b</sup>, Jie Wang<sup>a</sup>, Yan Li<sup>a</sup>, Xiaoxia Hu<sup>a</sup>, Junwen Yin<sup>a</sup>, Yeqing Peng<sup>a</sup>, Zhihao Li<sup>a</sup>,  
Yawen Li<sup>a</sup>, Baomin Li<sup>b</sup>, and Quan Yuan<sup>a,\*</sup>

<sup>a</sup>Key Laboratory of Analytical Chemistry for Biology and Medicine (Ministry of Education), College of Chemistry and Molecular Sciences, Wuhan University, Wuhan 430072, China

<sup>b</sup>School of Chemistry Engineering and Technology, China University of Mining and Technology, Xuzhou 221008, China

#### **Corresponding author**

\*Email: yuanquan@whu.edu.cn

## Chemicals

Tetraethyl orthosilicate (TEOS, Si>28.4%), chloroauric acid (HAuCl<sub>4</sub>·4H<sub>2</sub>O, Au>47.8%), nitrobenzene (C<sub>6</sub>H<sub>5</sub>NO<sub>2</sub>, >99%), azobenzene (C<sub>12</sub>H<sub>10</sub>N<sub>2</sub>, >97%), 4-nitrotoluene (C<sub>7</sub>H<sub>7</sub>NO<sub>2</sub>, CP), 4-chloronitrobenzene (C<sub>6</sub>H<sub>4</sub>ClNO<sub>2</sub>, CP), ethyl acetate (C<sub>4</sub>H<sub>8</sub>O<sub>2</sub>, >99.5%), methylbenzene (C<sub>7</sub>H<sub>8</sub>, ≥99.5%), isopropanol (C<sub>3</sub>H<sub>8</sub>O, CP), ammonium solution (NH<sub>3</sub>·H<sub>2</sub>O, 25%-28%), ethanol (C<sub>2</sub>H<sub>5</sub>OH, AR), cyclohexane (C<sub>6</sub>H<sub>12</sub>, AR), diethylene glycol (C<sub>4</sub>H<sub>10</sub>O<sub>3</sub>, >99%), cerium nitrate hexahydrate (Ce(NO<sub>3</sub>)<sub>3</sub>·6H<sub>2</sub>O, >99%), 2-(N-Morpholino) ethanesulfonic acid (MES, >99%), cetrimonium bromide (CTAB, ≥99.0%), polyvinylpyrrolidone (PVP, 1800), Sodium acetate anhydrous (CH<sub>3</sub>COONa, AR), phenylbenzene (C<sub>12</sub>H<sub>10</sub>, CP), potassium hydroxide (KOH, AR), and ammonium carbonate (NH<sub>4</sub>CO<sub>3</sub>, AR) were purchased from Sinopharm Chemical Reagent Co. (Shanghai China). Ammonium cerium (IV) nitrate ((NH<sub>4</sub>)<sub>2</sub>Ce(NO<sub>3</sub>)<sub>6</sub>, >99%) and 3-aminopropyltriethoxysilane (APTES, >98 %) were purchased from Sigma Aldrich. 1-ethyl-3-(3-dimethylaminopropyl) carbodiimide-HCl (EDC, >98%), N-hydroxysuccinimide (NHS, >98%), polyacrylic acid (PAA, MW 3000) and Ln<sub>2</sub>O<sub>3</sub> (Ln: Ho, Er, Tm, Yb, 99.99%) were obtained from Aladdin. Ln(NO<sub>3</sub>)<sub>3</sub> powder was prepared by dissolving corresponding lanthanide oxides in HNO<sub>3</sub>, and the solution was evaporated to get the solid powder. Stock solutions of Ln(NO<sub>3</sub>)<sub>3</sub> (0.2M) were prepared by dissolving the corresponding solid powder in DI water.

## Instruments

A JEOL JEM-2100 transmission electron microscopy (TEM, Japan) operated at 200 kV was used to characterize the size and morphologies of the prepared nanoparticles. Energy dispersive X-ray (EDX) and high-resolution TEM (HRTEM) analysis of the particles were also performed during TEM (JEOL, JEM-2100, Japan) measurements. The high-angle annular dark-field scanning transmission electron microscopy (HAADF-STEM) and elemental mapping were obtained on a TEM (JEOL ARM200F) equipped with probe forming Cs corrector and Gatan image filter (Quantum 965). Scanning electron microscope (SEM) characterization was performed on a Hitachi S-4800 microscope (Hitachi, Japan). Powder X-ray diffraction (XRD) patterns were recorded on a Bruker D8 X-ray diffractometer (Germany) with a Cu-K $\alpha$  radiation ( $\lambda = 1.5406 \text{ \AA}$ ). The scan was conducted from 10 ° to 80 ° with a speed of 4 °/min. All of the Fluorescence spectra were recorded on a Hitachi F-4600 spectrophotometer (Japan) equipped with a NIR laser (Shaanxi Kai Site Electronic Technology Co., Ltd, 980 nm, 5 W, China) which operated with a power of 5 W and the diameter of the NIR light spot was 1 cm. The UV-Vis spectra was recorded on a Shimadzu UV-2550 UV-Vis spectrometer (Japan). Fourier-transform infrared (FT-IR) spectra was collected on a Thermo Scientific Nicolet iS10 FT-IR spectrophotometer (USA) using KBr pellets. Zeta potential was measured by a Malvern Zetasizer Nano ZS (UK). A Nikon D3000 digital single-lens reflex camera (Japan) was used for recording photographs. The characterize absorption of TMB and ABTS were chartered by a Multiskan GO microplate reader (Thermo Scientific, America). Photocatalytic reactions were analyzed using a Shimadzu GC-MS (GCMS-QP2010 SE, Japan). Quantum yields measurement were conducted on a fluorescence spectroscopy (Edinburgh LFS920)

equipped with a NIR laser (BWT, DS2-11312-112, Beijing). An integrating sphere was used for measure the efficiency data, and an attenuation slice (Giai Photonics Co., Ltd.) for 980 nm laser was used to decrease the intensity of incident light. The power density of excitation light is 150 W/cm<sup>2</sup>.

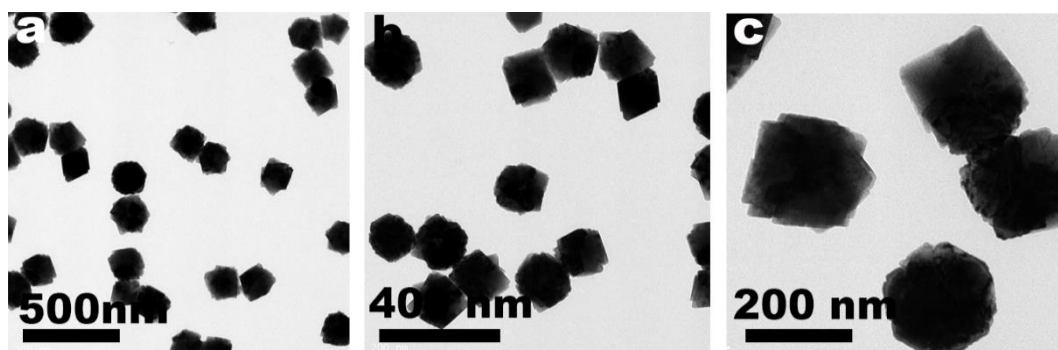


Figure S1. TEM images of o-CeO<sub>2</sub>.

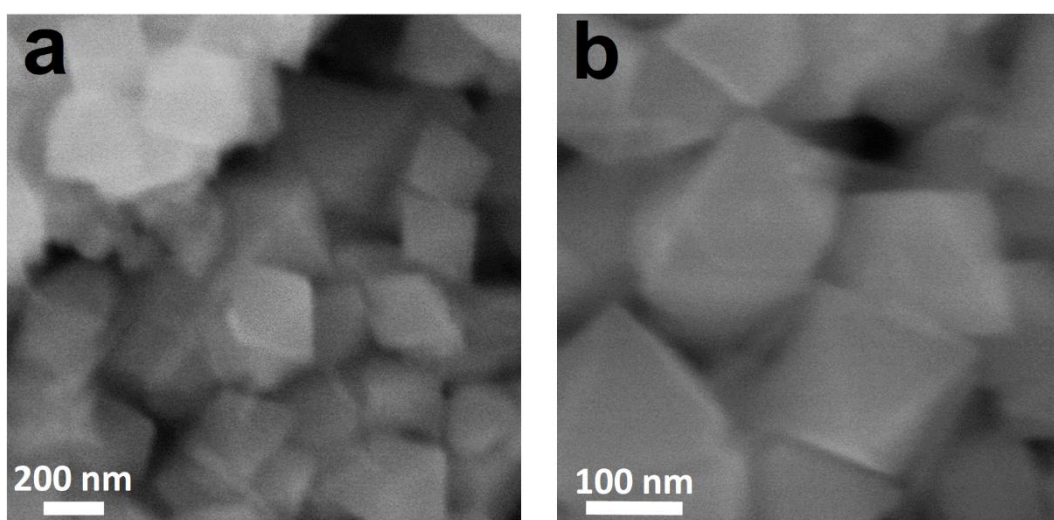


Figure S2. SEM images of o-CeO<sub>2</sub> nanoparticles at different magnifications.

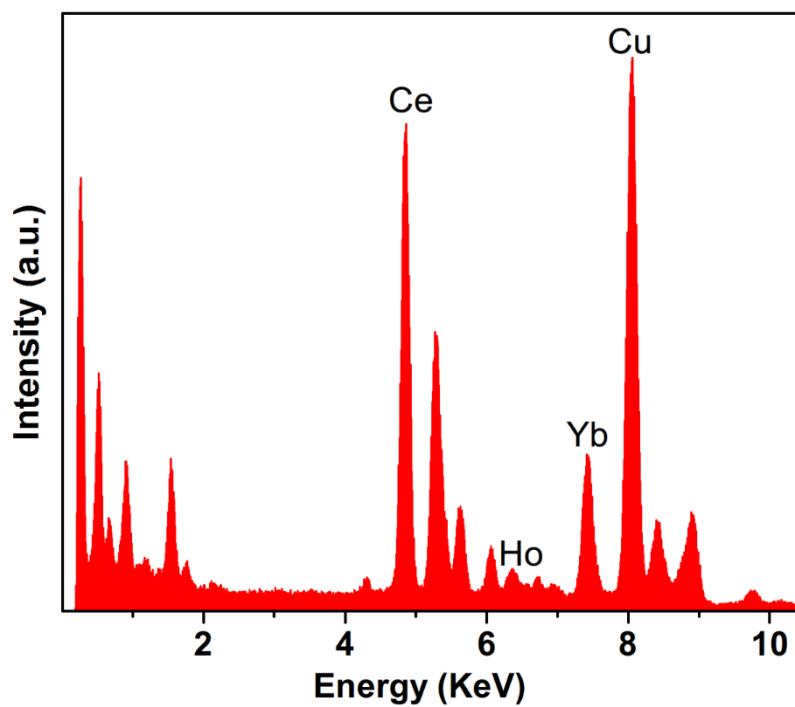


Figure S3. EDX analysis of o-CeO<sub>2</sub>:Yb<sup>3+</sup>/Ho<sup>3+</sup> nanoparticles.

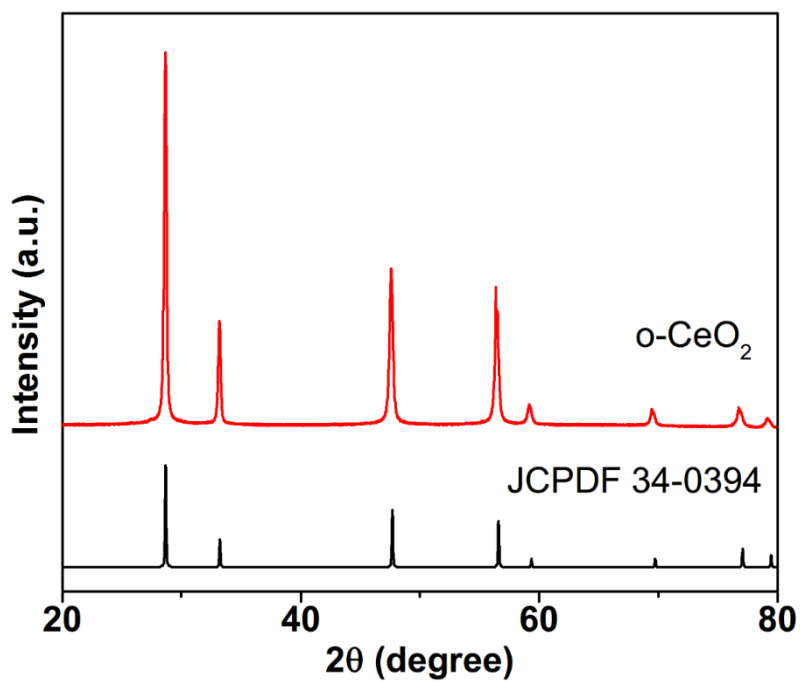


Figure S4. XRD pattern of lanthanide ions doped o-CeO<sub>2</sub> nanoparticles.

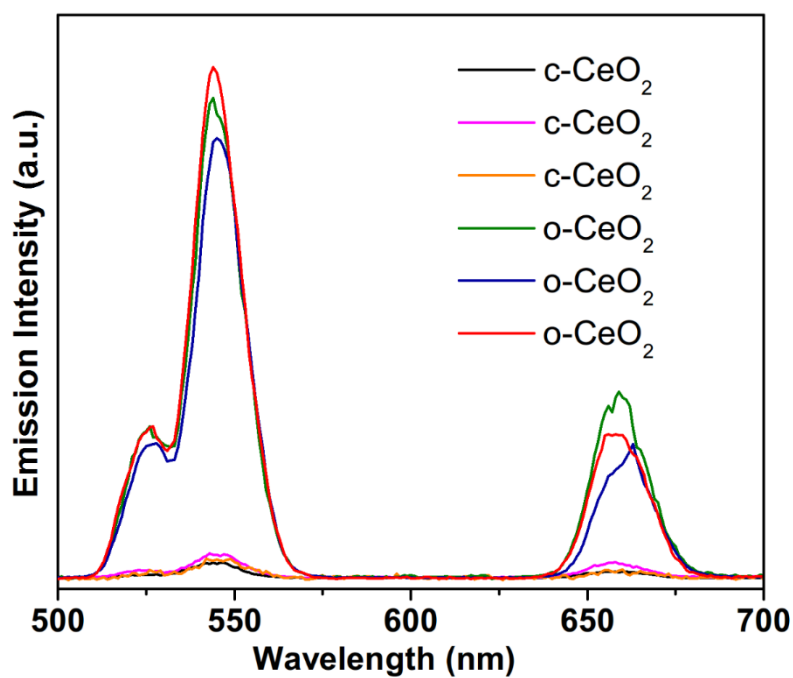


Figure S5. Upconversion luminescence spectra of lanthanide ions doped o-CeO<sub>2</sub> and c-CeO<sub>2</sub> nanoparticles.

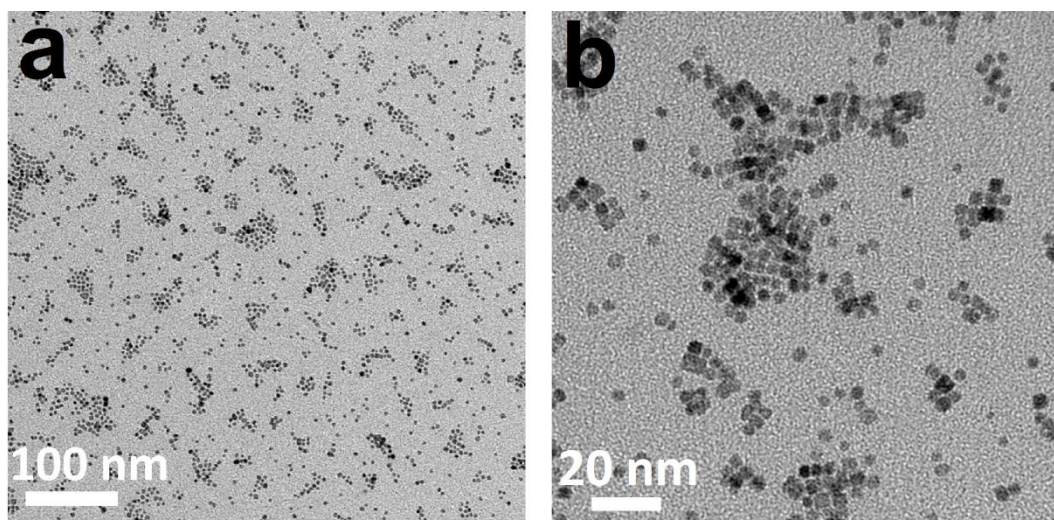


Figure S6. TEM images of c-CeO<sub>2</sub> at different magnifications.

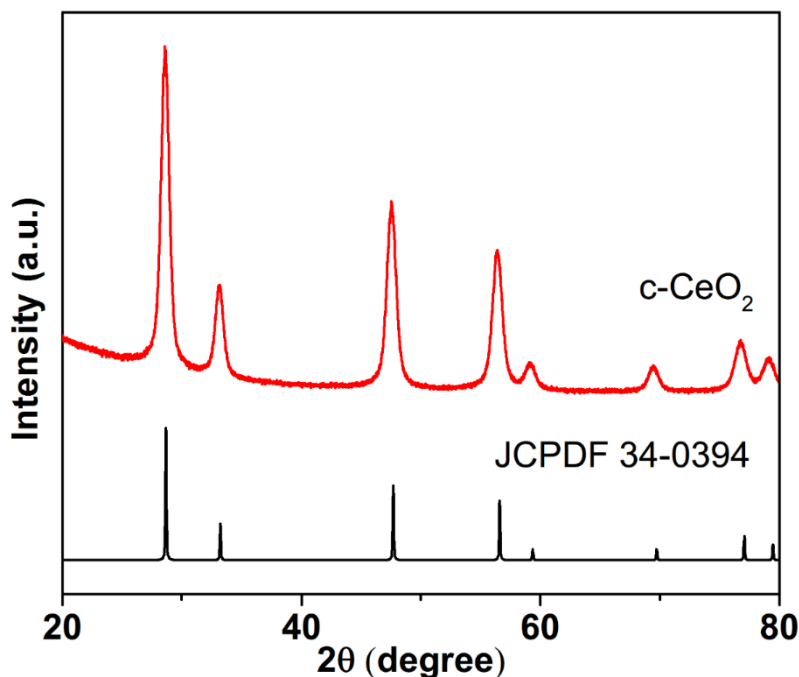
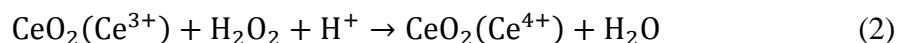
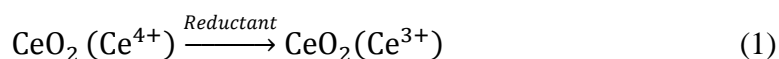


Figure S7. XRD pattern of c-CeO<sub>2</sub> nanoparticles.

### The pH-dependent oxidase-like activity of c-CeO<sub>2</sub>

One of the most charming properties of CeO<sub>2</sub> nanoparticles is the reversible redox cycles between Ce<sup>3+</sup> and Ce<sup>4+</sup> on their surface, which makes CeO<sub>2</sub> nanoparticles possess both reducibility and oxidizability. It is noteworthy that the reduction of Ce<sup>4+</sup> to Ce<sup>3+</sup> does not influence the structure of CeO<sub>2</sub> nanoparticles (Eq. 1 below) and the reduced Ce<sup>4+</sup> can be readily oxidized by oxidizers such as O<sub>2</sub> and H<sub>2</sub>O<sub>2</sub> to maintain the balance between Ce<sup>3+</sup> and Ce<sup>4+</sup> on the nanoparticles' surface (Eq. 2 below).<sup>1,2</sup> Therefore, researchers usually considered that CeO<sub>2</sub> nanoparticles have the oxidase-like activity.<sup>3-5</sup> In our experiment, TMB was also oxidized by Ce<sup>4+</sup> on the surface of CeO<sub>2</sub> nanoparticles.<sup>6</sup> In consideration that the structure of CeO<sub>2</sub> nanoparticles is not affected by the oxidization reaction and the reduced Ce<sup>4+</sup> could be further oxidized by oxidizers such as O<sub>2</sub> in the solution, thus it is reasonable to consider that the TMB is catalyzed by c-CeO<sub>2</sub> nanoparticles.



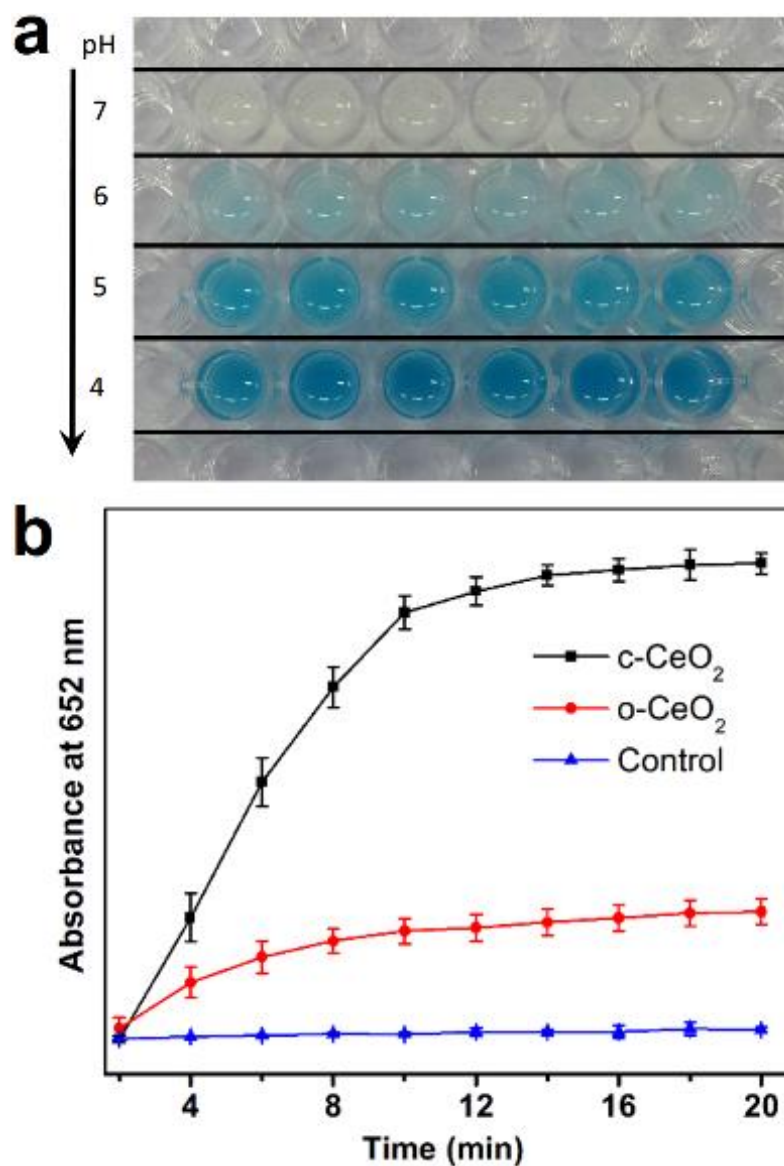


Figure S8. (a) Photograph of catalytic oxidization of TMB by c-CeO<sub>2</sub> nanoparticles at different pH values. (b) Comparison of the absorbance of TMB solutions catalyzed with different CeO<sub>2</sub> particle.

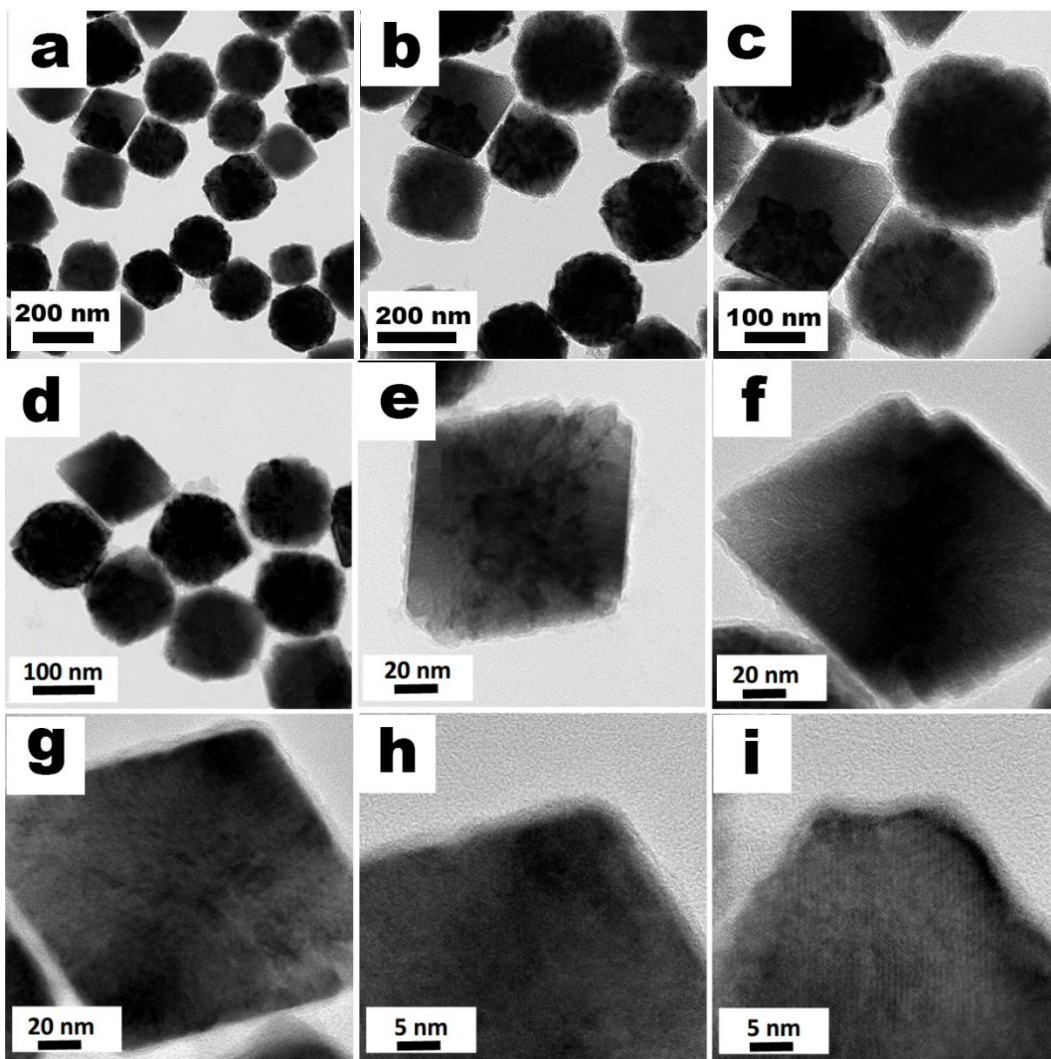


Figure S9. TEM images of  $o\text{-CeO}_2@SiO_2$  at different magnifications.

## Quantum yields of o-CeO<sub>2</sub> and o-CeO<sub>2</sub>@SiO<sub>2</sub>

The actual quantum yields (QY) of o-CeO<sub>2</sub> and o-CeO<sub>2</sub>@SiO<sub>2</sub> nanoparticles were quantified according to a method reported in previous study.<sup>7</sup> Specifically, NaYF<sub>4</sub>:20% Yb<sup>3+</sup>/2% Er<sup>3+</sup>@NaYF<sub>4</sub> core-shell nanoparticles with known QY is used as the reference sample. The upconversion QY is defined as the ratio of the number of the emitted upconverted photons to the number of the absorbed NIR photons (Eq. 3 below).

$$QY = \frac{\text{Photons Emitted}}{\text{Photons Absorbed}} = \frac{E}{A} \quad (3)$$

The QY of tested sample (QY<sub>S</sub>) and the reference sample (QY<sub>R</sub>) are given by:

$$QY_S = \frac{E_S}{A_S} \quad (4)$$

$$QY_R = \frac{E_R}{A_R} \quad (5)$$

Thus QY<sub>S</sub> can be calculated with:

$$QY_S = \left(\frac{E_S}{A_S}\right) \left(\frac{A_R}{E_R}\right) QY_R \quad (6)$$

As the QY<sub>R</sub> of the reference sample is 0.3% for the green emission under 980 nm excitation with 150 W/cm<sup>2</sup>,<sup>8</sup> the QY<sub>S</sub> can be given by the following formula:

$$QY_S = \left(\frac{E_S}{A_S}\right) \left(\frac{A_R}{E_R}\right) 0.3\% \quad (7)$$

The measurement were conducted on a fluorescence spectroscopy (Edinburgh LFS920) equipped with a NIR laser (BWT, DS2-11312-112, Beijing). An integrating sphere was used for measure the efficiency data, and an attenuation slice (Giai Photonics Co., Ltd.) for 980 nm laser was used to decrease the intensity of incident light. The power density of excitation light is 150 W/cm<sup>2</sup>. The characterization of the reference NaYF<sub>4</sub>:20% Yb<sup>3+</sup>/2% Er<sup>3+</sup>@NaYF<sub>4</sub> core-shell nanoparticles is shown in Figure S10. Figure S10a shows that the NaYF<sub>4</sub>:20% Yb<sup>3+</sup>/2% Er<sup>3+</sup> core is monodispersed with an average diameter of about 20 nm. After coated with the NaYF<sub>4</sub> shell, the diameter of the nanoparticles increases to about 30 nm (Figure S10b). The upconversion luminescence spectrum of the reference NaYF<sub>4</sub>:20% Yb<sup>3+</sup>/2% Er<sup>3+</sup>@NaYF<sub>4</sub> nanoparticles is shown in Figure S10c with the characteristic green emission at around 550 nm. According to Eq. 7, the quantum yields of o-CeO<sub>2</sub> and o-CeO<sub>2</sub>@SiO<sub>2</sub> nanoparticles were determined to be 0.028% and 0.053% respectively, suggesting that the silica shell can improve the quantum yields of CeO<sub>2</sub>-based upconversion nanoparticles.

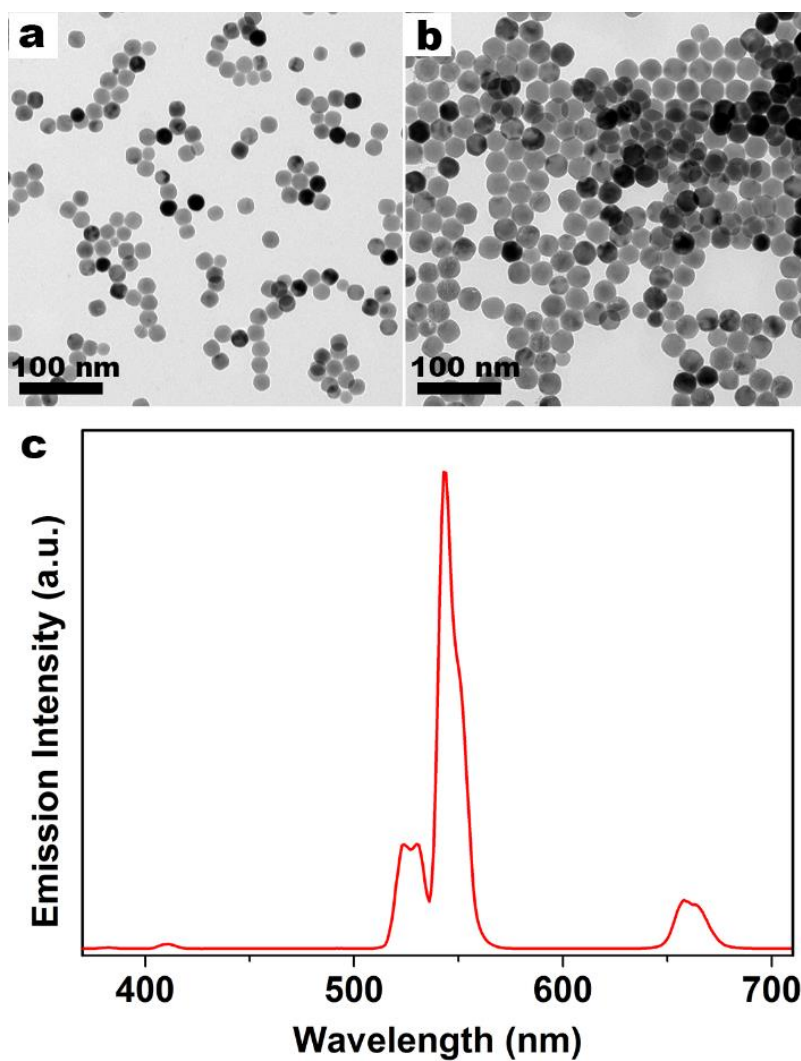


Figure S10. TEM images of  $\text{NaYF}_4:20\% \text{Yb}^{3+}/2\% \text{Er}^{3+}$  (a) and  $\text{NaYF}_4:20\% \text{Yb}^{3+}/2\% \text{Er}^{3+}@\text{NaYF}_4$  (b) nanoparticles. (c) Upconversion luminescence spectrum of  $\text{NaYF}_4:20\% \text{Yb}^{3+}/2\% \text{Er}^{3+}@\text{NaYF}_4$  nanoparticles.

## The relationship between upconversion intensity versus pump power

According to previous study,<sup>9,10</sup> the upconversion emission intensity ( $I_{EM}$ ) is proportional to the  $n$ th power of the NIR pump intensity ( $I_{NIR}$ ):

$$I_{EM} \propto I_{NIR}^n \quad (8)$$

Where  $n$  is the number of the absorbed pump photons.

To investigate the upconversion mechanism, the pump power dependences of upconversion emissions in o-CeO<sub>2</sub> and o-CeO<sub>2</sub>@SiO<sub>2</sub> were measured and the results are displayed in Figure S11. The emission peaks of o-CeO<sub>2</sub> nanoparticles at 543, 554 and 673 nm are attributed to the <sup>5</sup>F<sub>4</sub>→<sup>5</sup>I<sub>8</sub>, <sup>5</sup>S<sub>2</sub>→<sup>5</sup>I<sub>8</sub> and <sup>5</sup>F<sub>5</sub>→<sup>5</sup>I<sub>8</sub> transition of Ho<sup>3+</sup> respectively (Figure S11a). The intensities of the above emission peaks increase gradually with the increase of the pump power of the NIR light. Figure S11c shows the pump power dependence of upconversion emission in the o-CeO<sub>2</sub> nanoparticles. The slope value represents the number of pump photons absorbed ( $n$ ) per short wavelength photon emitted.<sup>11</sup> The values of slope are determined to be 1.88, 1.92 and 1.78 for emissions at 543, 554 and 673 nm, respectively. These values are between 1 and 2, suggesting a two-photon upconversion mechanism is involved to generate the above emissions in o-CeO<sub>2</sub> nanoparticles. As for o-CeO<sub>2</sub>@SiO<sub>2</sub>, a similar upconversion behavior is observed, as shown in Figure S11b and S11d. The values of slope are 1.83, 1.85 and 1.73 for emissions at 543, 554 nm and 673 nm respectively, which also indicates the two-photon upconversion process for all of the above emissions.

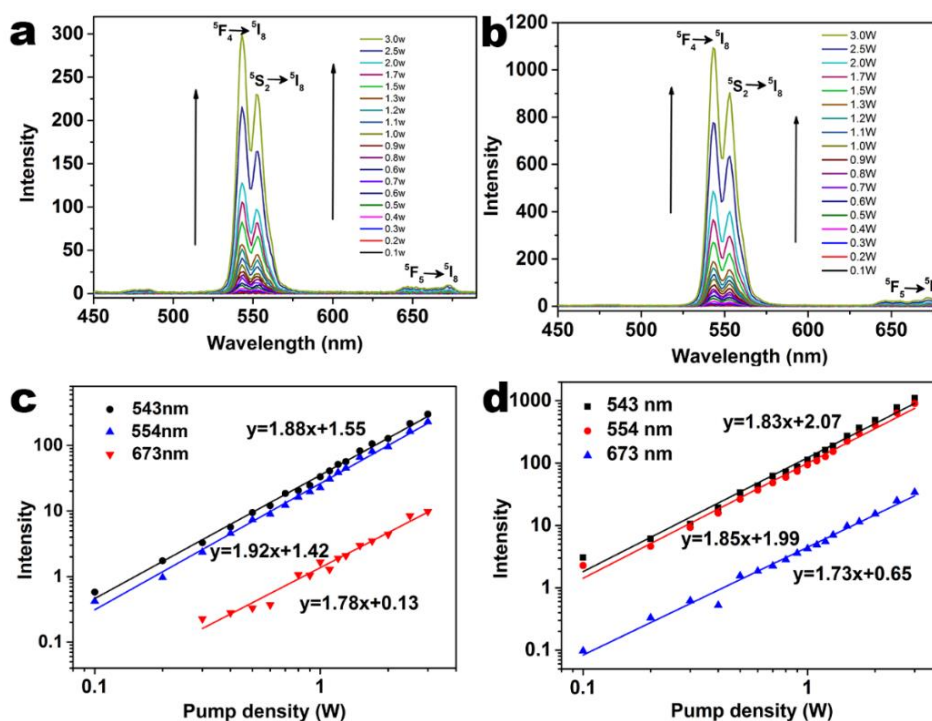


Figure S11. Upconversion luminescence spectra of (a) o-CeO<sub>2</sub> and (b) o-CeO<sub>2</sub>@SiO<sub>2</sub> under excitation of different pump power. Pump power dependences of upconversion emissions in (c) o-CeO<sub>2</sub> and in (d) o-CeO<sub>2</sub>@SiO<sub>2</sub>.

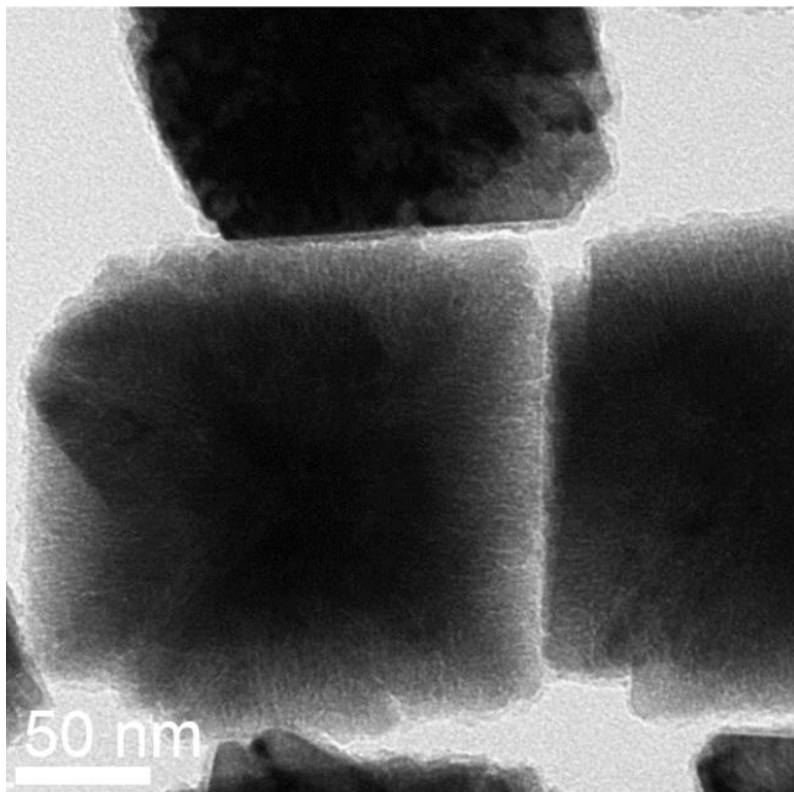


Figure S12. TEM image of amino groups modified  $o\text{-CeO}_2@SiO_2$ .

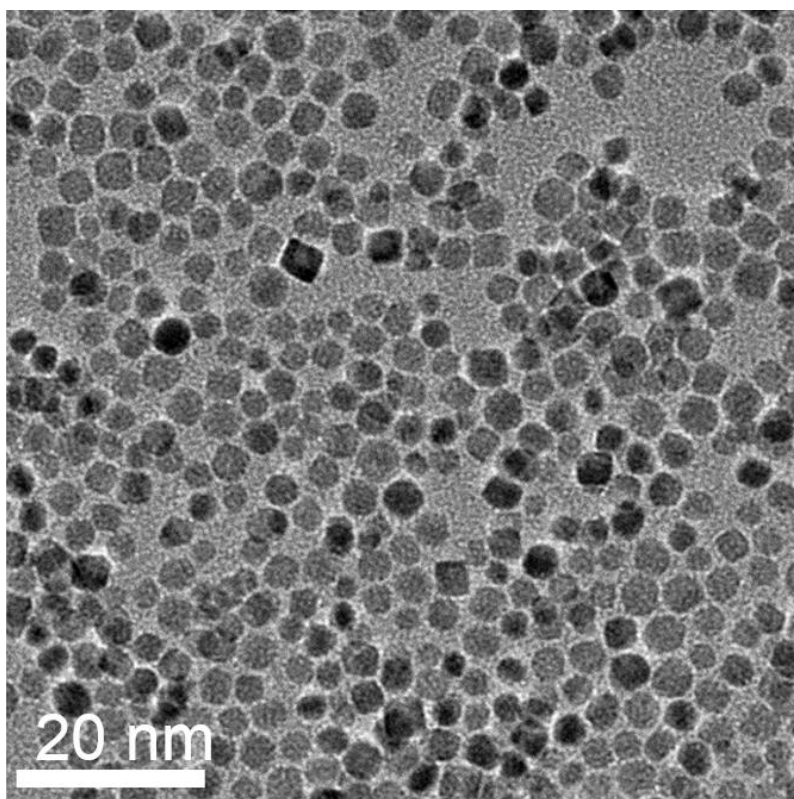


Figure S13. TEM image of  $c\text{-CeO}_2\text{-COOH}$ .

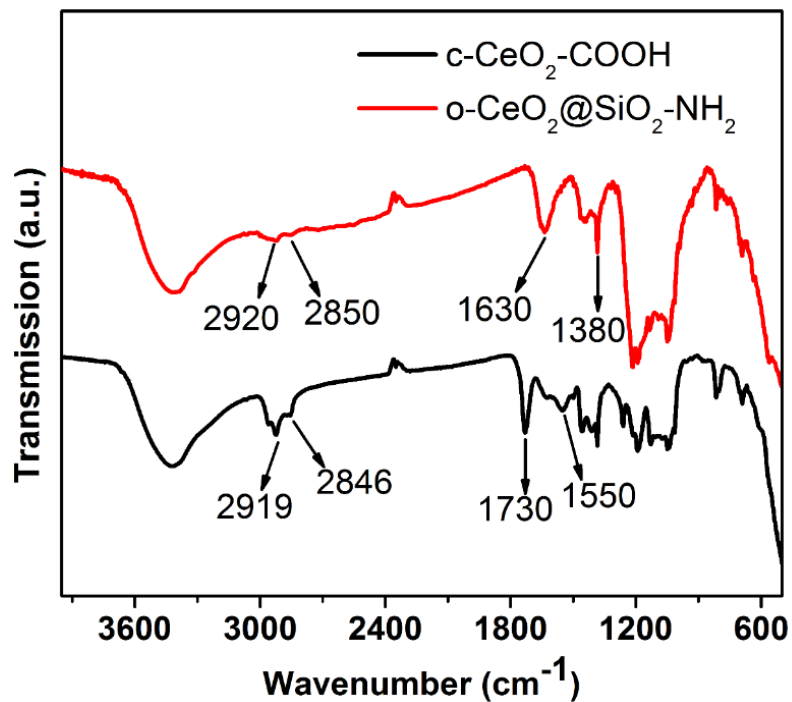


Figure S14. FTIR absorption spectra of c-CeO<sub>2</sub>-COOH and o-CeO<sub>2</sub>@SiO<sub>2</sub>-NH<sub>2</sub>.

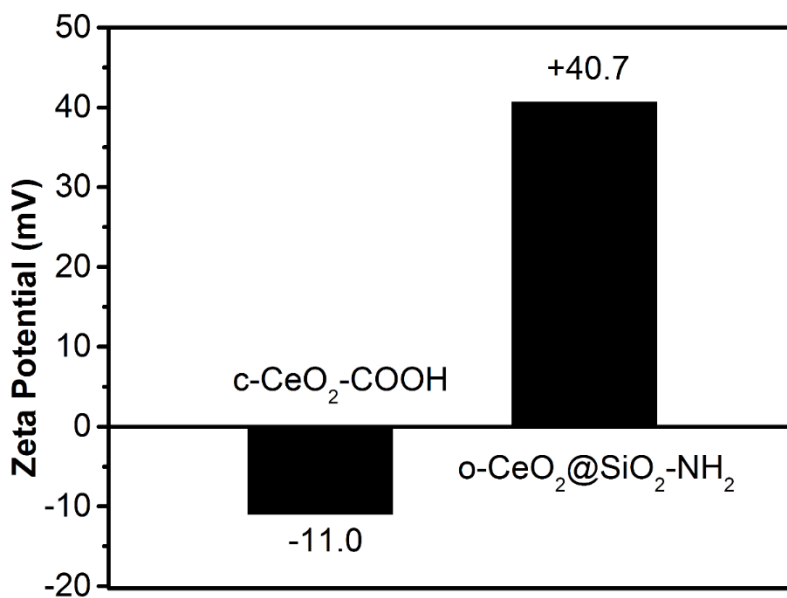


Figure S15. Zeta potentials of c-CeO<sub>2</sub>-COOH and o-CeO<sub>2</sub>@SiO<sub>2</sub>-NH<sub>2</sub> nanoparticles.

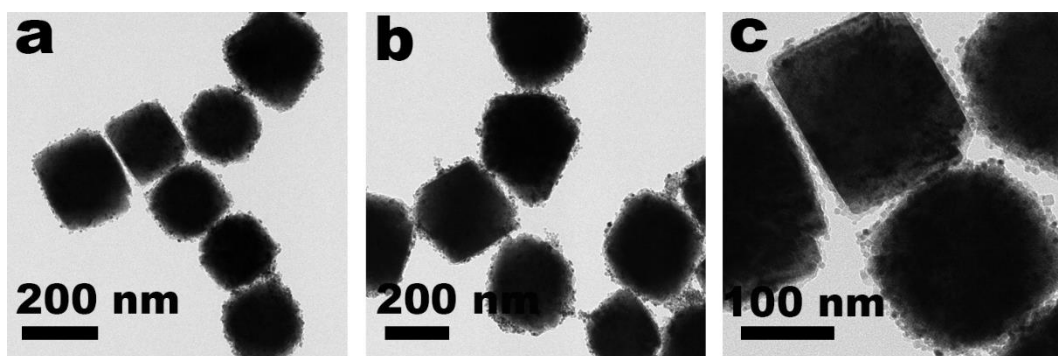


Figure S16. TEM images of o-CeO<sub>2</sub>@SiO<sub>2</sub>@c-CeO<sub>2</sub>.

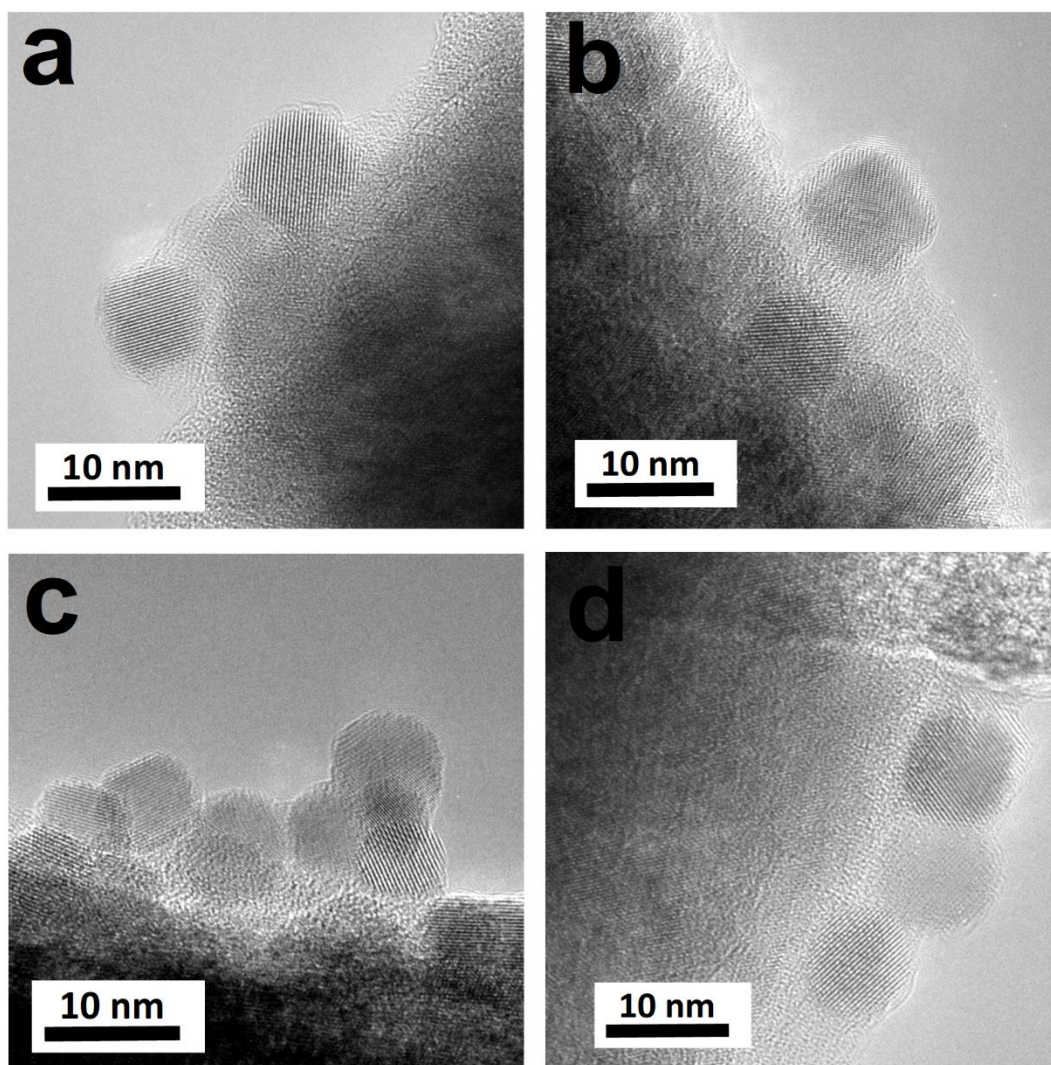


Figure S17. HRTEM images of o-CeO<sub>2</sub>@SiO<sub>2</sub>@c-CeO<sub>2</sub> nanoparticles.

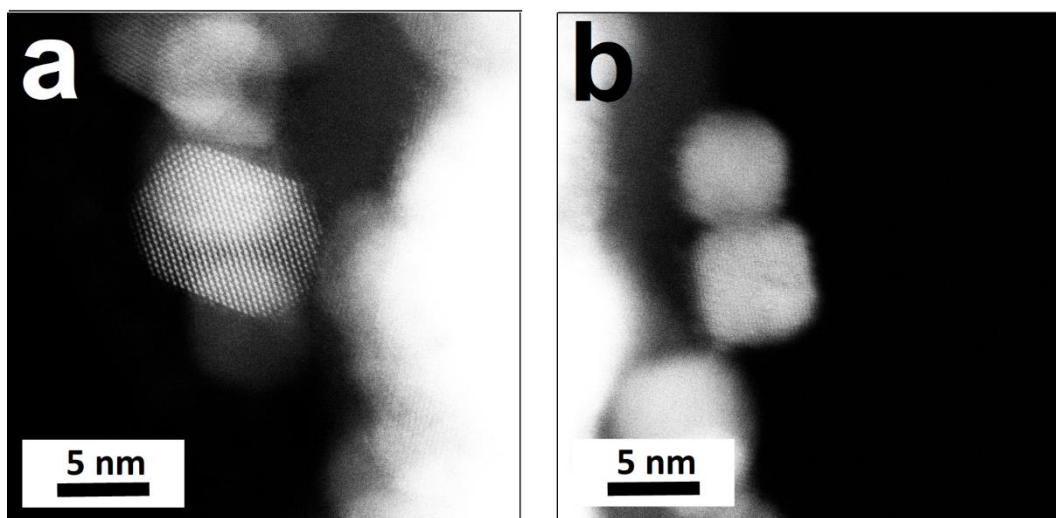


Figure S18. HADDF-STEM images of o-CeO<sub>2</sub>@SiO<sub>2</sub>@c-CeO<sub>2</sub> nanoparticles.

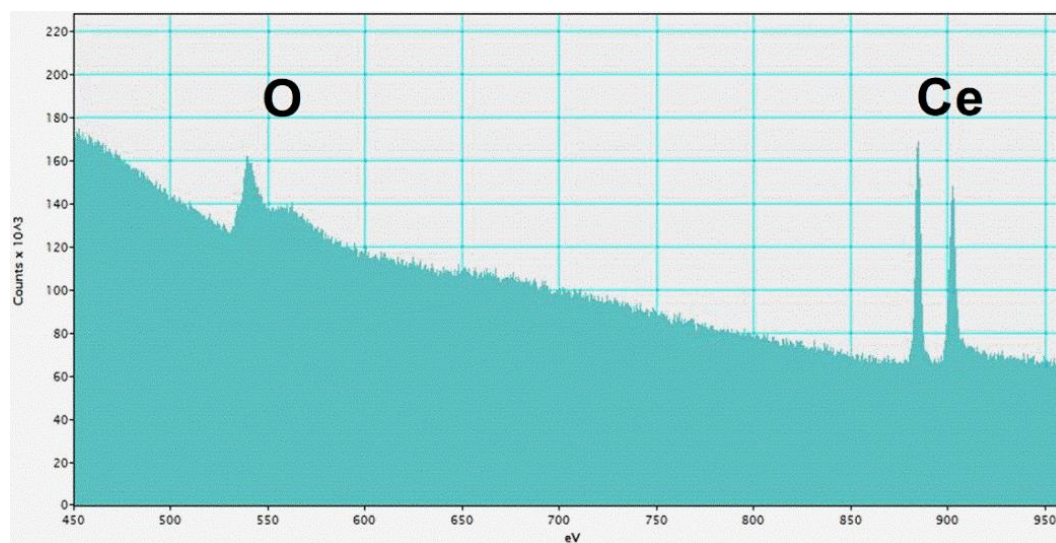


Figure S19. Electron Energy Loss Spectroscopy (EELS) of the outside c-CeO<sub>2</sub> in the core-shell-satellite structure.

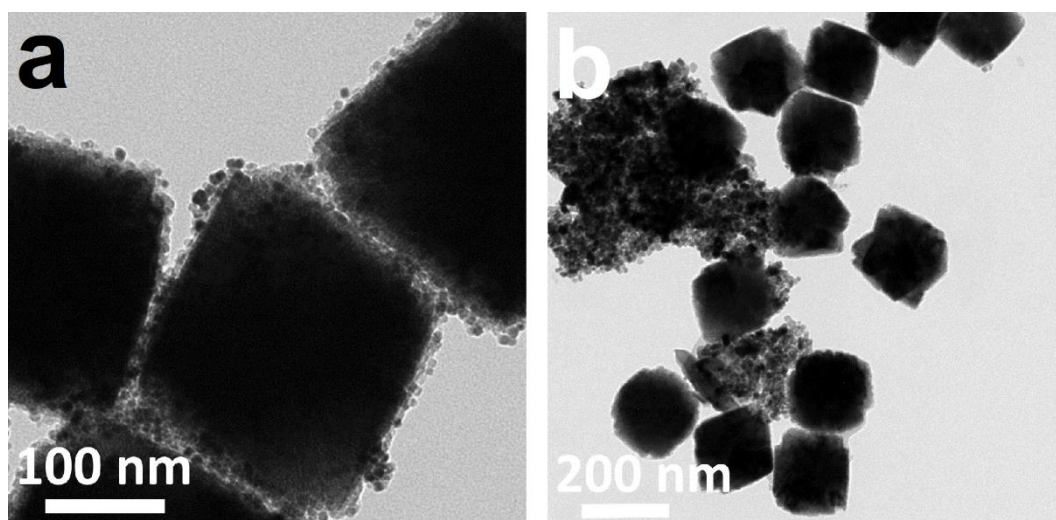


Figure S20. (a) TEM image of o-CeO<sub>2</sub>@SiO<sub>2</sub>@c-CeO<sub>2</sub> nanoparticles prepared with o-CeO<sub>2</sub>-NH<sub>2</sub> and c-CeO<sub>2</sub>-COOH. (b) TEM image of nanoparticles prepared with unmodified o-CeO<sub>2</sub> and c-CeO<sub>2</sub>-COOH.

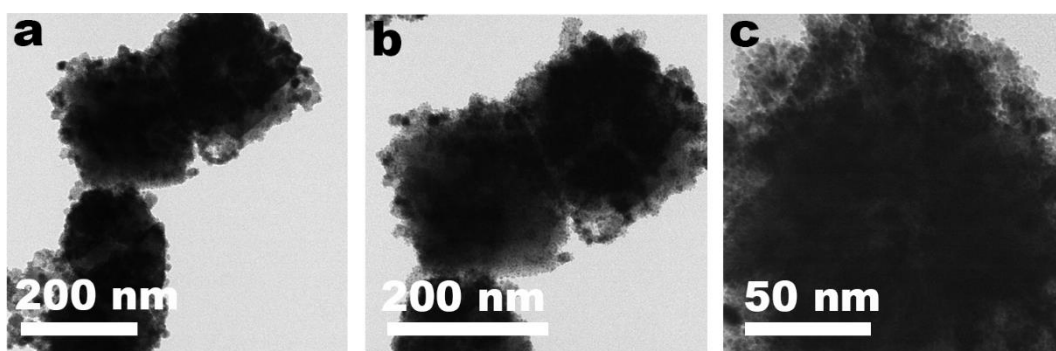


Figure S21. TEM images of o-CeO<sub>2</sub>@SiO<sub>2</sub>@c-CeO<sub>2</sub>/Au.

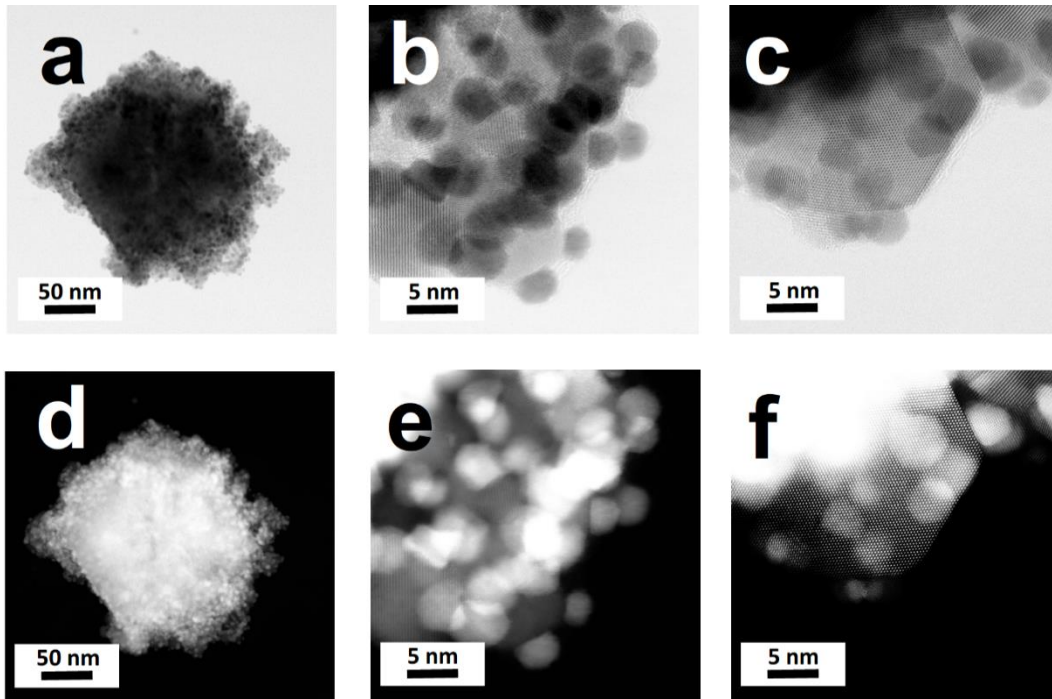


Figure S22. TEM (a) and HRTEM (b and c) images of o-CeO<sub>2</sub>@SiO<sub>2</sub>@c-CeO<sub>2</sub>/Au. HAADF-STEM (d) and HRHAADF-STEM (e and f) images of o-CeO<sub>2</sub>@SiO<sub>2</sub>@c-CeO<sub>2</sub>/Au.

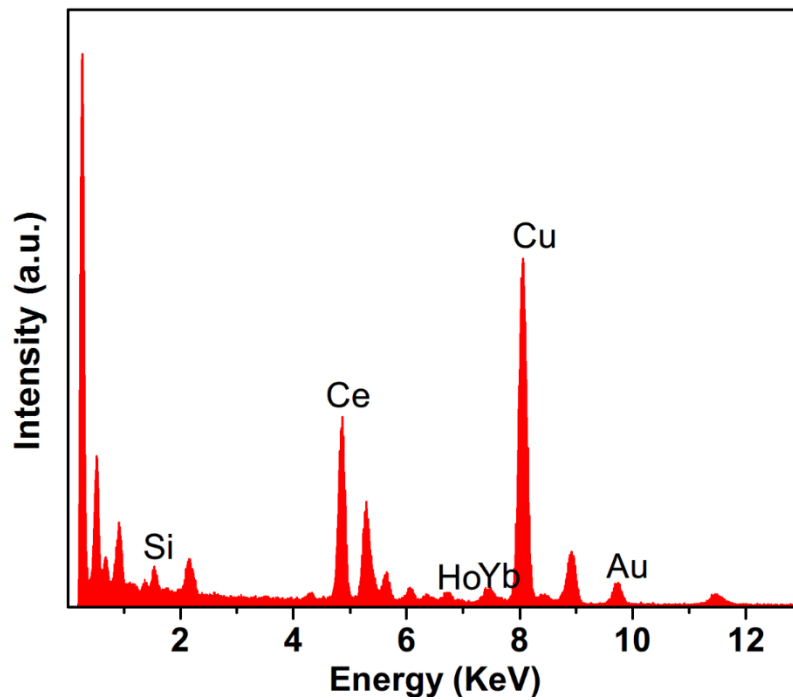


Figure S23. EDX analysis of o-CeO<sub>2</sub>@SiO<sub>2</sub>@c-CeO<sub>2</sub>/Au.

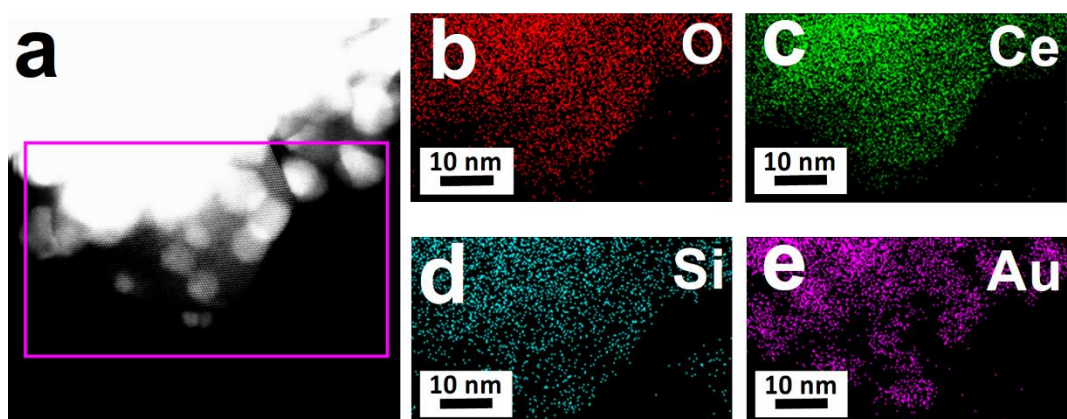


Figure S24. (a) HAADF-STEM of  $o\text{-CeO}_2@SiO_2@c\text{-CeO}_2/Au$ . (b-e) Elemental mapping images of O, Ce, Si and Au on the nanostructure shown in (a) respectively.

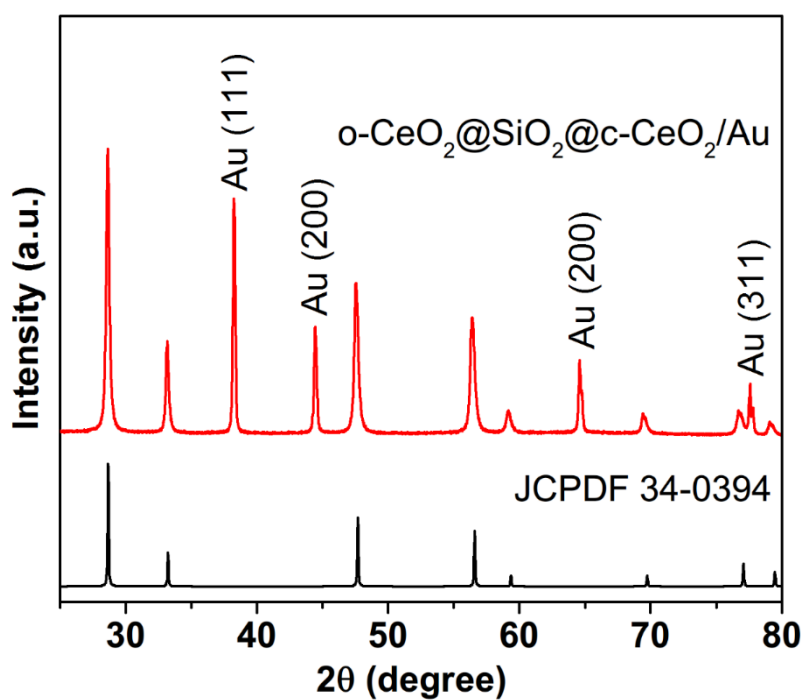


Figure S25. XRD pattern of  $o\text{-CeO}_2@SiO_2@c\text{-CeO}_2/Au$ .

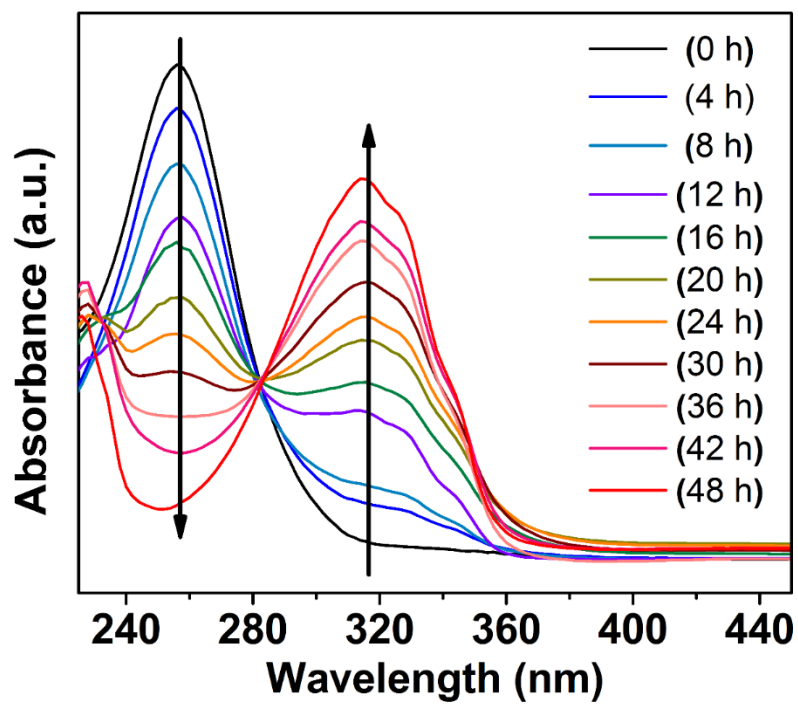


Figure S26. The absorbance of nitrobenzene solution catalyzed with  $o\text{-CeO}_2@SiO_2@c\text{-CeO}_2/Au$  under NIR light irradiation at different time intervals.

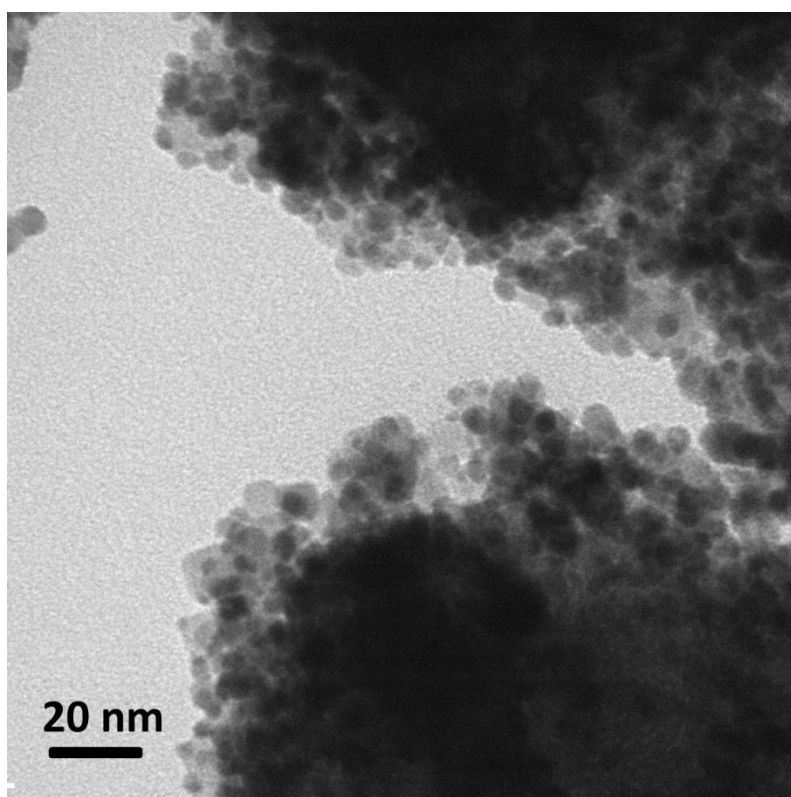


Figure S27. TEM image of  $o\text{-CeO}_2@SiO_2-c\text{-CeO}_2/Au$  after the 4th cycles.

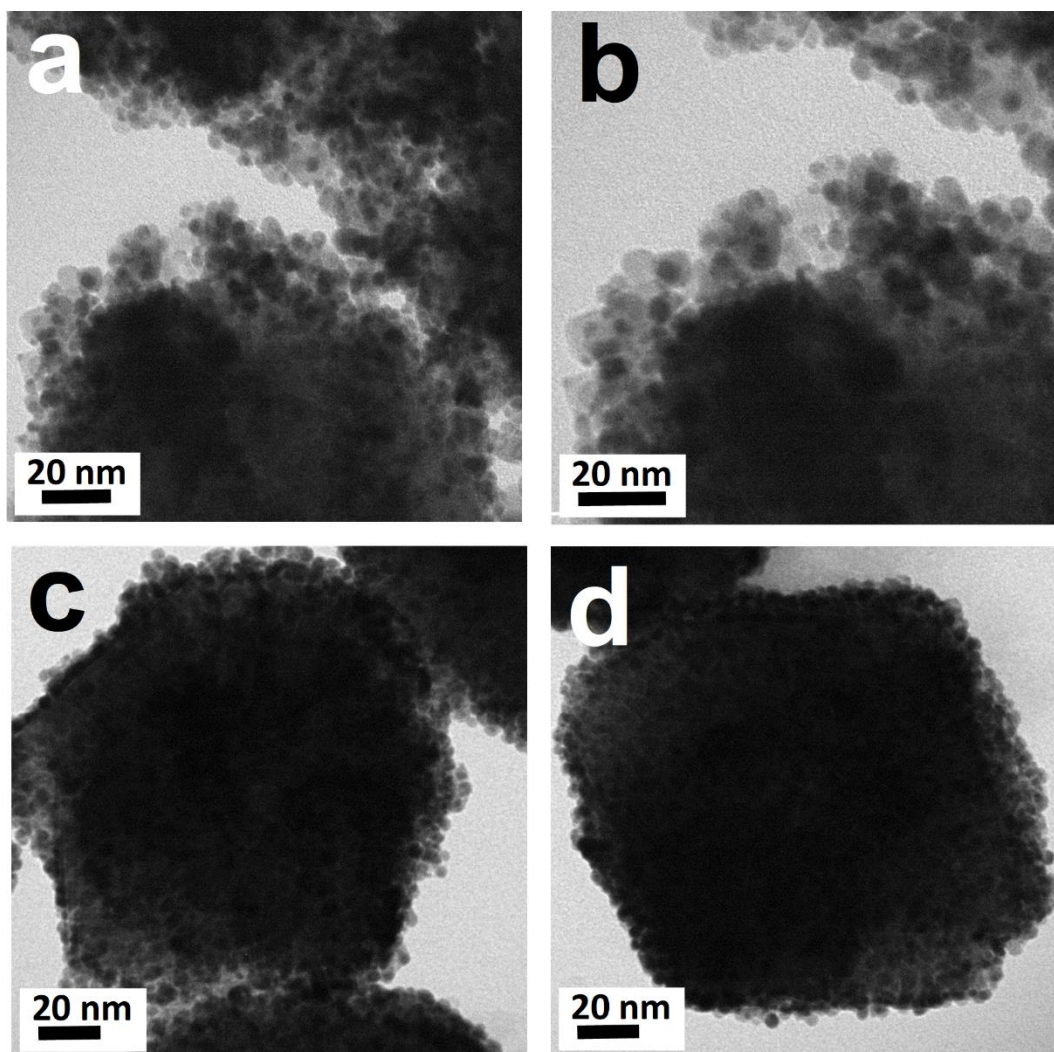


Figure S28. (a, b) TEM images of  $o\text{-CeO}_2@SiO_2@c\text{-CeO}_2/Au$ . (c, d) TEM images of  $o\text{-CeO}_2@SiO_2/Au$ .

Table S1. Control experiments of different kind of catalysts in NIR-driven photocatalysis of nitrobenzene (Conv.=conversion, Selec.=selectivity)

catalyst	T [°C]	t [h]	Conv. [%]	Selec. [%]
$o\text{-CeO}_2@SiO_2$	40	48	/	/
$o\text{-CeO}_2@SiO_2\text{-c-CeO}_2$	40	48	/	/
$o\text{-CeO}_2@SiO_2/Au$	40	48	33.41	70.92
$o\text{-CeO}_2@SiO_2\text{-c-CeO}_2+Au$	40	48	39.30	72.59
$o\text{-CeO}_2@SiO_2\text{-c-CeO}_2/Au$	40	48	99.60	98.17

## Application explorations of core-shell-satellites

Apart from the potential applications in bioimaging and sensing, the core-shell-satellite nanoparticles can be further applied in areas such as preventing counterfeiting and indicating the progress of chemical reactions. For preventing counterfeiting, the core-shell-satellite nanostructure can be utilized for the preparation of near-infrared ink. The pattern typed on the logo of the goods with this near-infrared ink cannot be seen with naked eyes under natural light. However, when NIR light is applied, the pattern on the logo can be clearly seen. Thus one can see that the core-shell-satellite nanoparticles holds great promise for preventing counterfeiting.

As for indicating the progress of chemical reactions, assuming that the substrates or the products of the chemical reaction catalyzed by the core-shell-satellite based catalyst possess absorption at 543, 554 or 673 nm, the emission of the core-shell-satellite nanostructure will be quenched by the substrates or the products. On the one hand, if the substrates can quench the emission of the core-shell-satellite nanostructure, the consumption of the substrates will leads to the increase of the luminescence intensity of the reaction solution. On the one hand, if the products can quench the emission of the core-shell-satellite nanostructure, the accumulation of the products will gradually decrease the luminescence intensity of the reaction solution. From the above analysis, one can clearly see that the core-shell-satellite nanoparticles can find applications beyond bioimaging and sensing. We have added this application explorations to the supporting information of the revised manuscript.

## Reference

1. Heckert, E. G.; Karakoti, A. S.; Seal, S.; Self, W. T., The Role of Cerium Redox State in the SOD Mimetic Activity of Nanoceria. *Biomaterials* **2008**, *29*, 2705-2709.
2. Lin, Y. H.; Xu, C.; Ren, J. S.; Qu, X. G., Using Thermally Regenerable Cerium Oxide Nanoparticles in Biocomputing to Perform Label-Free, Resettable, and Colorimetric Logic Operations. *Angew. Chem. Int. Ed.* **2012**, *51*, 12579-12583.
3. Asati, A.; Santra, S.; Kaittanis, C.; Nath, S.; Perez, J. M. Oxidase-Like Activity of Polymer-Coated Cerium Oxide Nanoparticles. *Angew. Chem. Int. Ed.* **2009**, *48*, 2308-2312.
4. Kim, M. I.; Park, K. S.; Park, H. G., Ultrafast Colorimetric Detection of Nucleic Acids Based on the Inhibition of the Oxidase Activity of Cerium Oxide Nanoparticles. *Chem. Commun.* **2014**, *50*, 9577-9580.
5. Asati, A.; Kaittanis, C.; Santra, S.; Perez, J. M.; pH-Tunable Oxidase-Like Activity of Cerium Oxide Nanoparticles Achieving Sensitive Fluorogenic Detection of Cancer Biomarkers at Neutral pH. *Anal. Chem.* **2011**, *83*, 2547-2553.

6. Jiao, X.; Song, H. J.; Zhao, H. H.; Bai, W.; Zhang, L. C.; Lv, Y., Well-Redispersed Ceria Nanoparticles: Promising Peroxidase Mimetics for H<sub>2</sub>O<sub>2</sub> and Glucose Detection. *Anal. Methods* **2012**, *4*, 3261-3267.
7. Chen, G. Y.; Ohulchanskyy, T. Y.; Kachynski, A.; Ågren, H.; Prasad, P. N. Intense Visible and Near-Infrared Upconversion Photoluminescence in Colloidal LiYF<sub>4</sub>:Er<sup>3+</sup> Nanocrystals under Excitation at 1490 nm. *ACS Nano* **2011**, *5*, 4981-4986.
8. Boyer, J.-C. Veggel, F. C. J. M. Absolute Quantum Yield Measurements of Colloidal NaYF<sub>4</sub>: Er<sup>3+</sup>, Yb<sup>3+</sup> Upconverting Nanoparticles. *Nanoscale* **2012**, *2*, 1417-1419.
9. Cho, J.-H.; Bass, M.; Babu, S.; Dowding, J. M.; Self, W. T.; Seal, S., Up Conversion Luminescence of Yb<sup>3+</sup>-Er<sup>3+</sup> Codoped CeO<sub>2</sub> Nanocrystals with Imaging Applications. *J. Lumin.* **2012**, *132*, 743-749.
10. Chen, G. Y.; Liu, H. C.; Somesfalean, G.; Liang, H. J.; Zhang, Z. G., Upconversion Emission Tuning from Green to Red in Yb<sup>3+</sup>/Ho<sup>3+</sup>-Codoped NaYF<sub>4</sub> Nanocrystals by Tridoping with Ce<sup>3+</sup> ions. *Nanotechnology* **2009**, *20*, 3008-3013.
11. Dong, H.; Sun, L.-D.; Yan, C.-H. Basic Understanding of the Lanthanide Related Upconversion Emissions. *Nanoscale* **2013**, *5*, 5703-5714.